coatings

MDPI

Article

# Corrosion Resistance of Al/SiC Laser Cladding Coatings on AA6082

**Ainhoa Riquelme *, Pilar Rodrigo, María Dolores Escalera-Rodríguez and Joaquín Rams**

Ciencia e Ingeniería de Materiales, Escuela Superior de Ciencias Experimentales y Tecnología, Universidad Rey Juan Carlos, Móstoles, 28933 Madrid, Spain; pilar.rodrigo@urjc.es (P.R.); dolores.escalera@urjc.es (M.D.E.-R.); joaquin.rams@urjc.es (J.R.)

* Correspondence: ainhoa.riquelme.aguado@urjc.es

Received: 11 June 2020; Accepted: 11 July 2020; Published: 14 July 2020


**Abstract:** Aluminum matrix composites reinforced with silicon carbide particles ($SiC_p$) were deposited by laser cladding on AA6082 aluminum alloy. Different compositions of the matrix of the composites coating were used and different amounts of Si and Ti were added to a base of Al-12Si in order to control the reactivity between molten aluminum and $SiC_p$ during laser cladding. The corrosion behavior of the coatings deposited was evaluated in 3.5 wt.% NaCl solution using gravimetric analyses and electrochemical polarization tests. The corrosion products observed were $Al(OH)_3$ and $Al_2O_3$, and they formed a layer that limited the evolution of corrosion. However, the presence of discontinuities in it reduced the corrosion resistance of the coating. The corrosion mechanisms were different depending on the coating composition. The addiction of Ti to the alloy allowed for better corrosion behavior for the composite coating than that of the aluminum substrate.

**Keywords:** laser cladding; aluminum matrix composites; SiC particles; silicon; titanium

## 1. Introduction

The need of weight reduction and increased mechanical properties, mainly in aerospace and automobile sectors, have stimulated engineers to develop new material combinations with high mechanical properties [1,2]. Aluminum matrix composites reinforced with SiC particles ($SiC_p$) have better tribological properties than the equivalent alloys [3,4]. The possibility of fabricating Al/$SiC_p$ coatings on aluminum could be a possible solution to obtain light components with high tribological properties [5–8]. However, the incorporation of a ceramic phase into an aluminum matrix can change its corrosion behavior. Several factors determine the corrosion behavior of metal-matrix composites such as the composition of the matrix alloy and its microstructure, the reinforcement dispersion and the technique used to fabricate the composite [9].

Laser cladding is an effective fabrication process to obtain composite coatings as it provides compact coatings with high adhesion to the substrates and it also has a very high versatility [10,11]. For the formulation of Al/$SiC_p$, it is a very interesting process because it allows a direct interaction of SiC particles and molten aluminum at a controlled temperature. However, it is known that between 667 °C and 1347 °C, Al and $SiC_p$ react and dissolve the reinforcing $SiC_p$, while Si and $Al_4C_3$ are formed. Particularly, the $Al_4C_3$ formation must be avoided because it is a brittle and hygroscopic intermetallic, and it strongly degrades the properties of the composite [12–17].

In previous research, laser cladding with Al/$SiC_p$ on aluminum alloys were successfully carried out [18,19], and the effect of the addition of other alloying elements (silicon and titanium) to the matrix of the composite coating was investigated [20]. The addition of silicon into the Al matrix displaces the reaction between Al and $SiC_p$ to the products, inhibiting the aluminum carbide formation [21–23] and, therefore, reducing the degradation of the silicon carbide particles. For the cladding processes,

it is needed the addition of at least 40 wt.% Si in the Al/$SiC_p$ composite matrix to inhibit the $Al_4C_3$ formation. The microstructure of this coating consists in an Al-Si hypereutectic matrix reinforced with undegraded SiC particles [20]. Also, the addition of 20 wt.% Ti avoided the presence of $Al_4C_3$ in the composite matrix. In this case, the avidity of Ti to C and Si favored the formation of TiC and $TiSi_2$ instead of producing other carbides [24–26]. The main advantage of the modified systems is that the new phases formed are not harmful, and they even act as hardening elements, so that they also contribute to the composite as an in-situ precipitated reinforcement [1].

Present study describes and compares the corrosion resistance of AA6082 aluminum alloy with that of some Al/$SiC_p$ composite coatings with different compositions deposited on an AA6082 in 3.5 wt.% NaCl solution at room temperature. The strategies used for avoiding the degradation of the reinforcement were the addition of 40 wt.% Si and of 20 wt.% Ti. The evolution of the corrosion behavior with immersion time has been studied and different corrosion mechanisms have been proposed.

## 2. Materials and Methods

Coatings were deposited on 30 × 30 × 5 $mm^3$ AA6082 coupons with a T6 treatment were supplied by Fundiciones Gómez (La Rioja, Spain). The main alloying elements of the AA6082 were (in wt.%): 1.05 Si; 0.23 Fe; 0.03 Cu; 0.57 Mg, 0.57 Mn; 0.02 Zn; 0.02 Ti, and balance Al. The surface of the substrates was prepared by blasting using brown corundum (D50 = 60 μm) for 1 min. For the cladding process, commercial powder of aluminum, silicon carbide, silicon and titanium (Table 1) were mixed on a ball mill for 5 h with different proportions in order to obtain different composite powders (Table 2).

**Table 1.** Powders properties and suppliers.

| Product | Supplier | D50 (μm) | ρ (g·cm$^{-3}$) |
|---|---|---|---|
| Al 12 wt.% Si | Metco 52C-NS | 71 | 2.7 |
| SiC | Navarro S.A F-360 | 26.2 | 2–2.3 |
| Si | Alfa Aesar | 44 | 2.3 |
| Ti | Alfa Aesar | 100 | 4.5 |

**Table 2.** Cladding powder proportions.

| Percentage | Abbreviated Name |
|---|---|
| Al 12 wt.% Si—30 wt.% SiC | Al 12Si/SiC |
| Al 40 wt.% Si—30 wt.% SiC | Al 40Si/SiC |
| Al 12Si wt.%—20 wt.% Ti—30 wt.% SiC | Al 12Si 20Ti/SiC |

The coatings were prepared by laser cladding using a 1300 W and 808–940 nm wavelength continuous wave diode laser (ROFIN DL013S, Santa Clara, CA, USA) connected to an ABB IRB2400 robot (Asea Brown Boveri, Zurich, Switzerland). The powder was sprayed coaxially to the laser beam trough a coaxial nozzle (Fraunhofer IWS COAX 8, Fraunhofer Institute for Material and Beam Technology, Winterbergstraße, Dresden, Germany). The processing parameters were set on preliminary research and Table 3 shows the laser control parameters used during the test.

**Table 3.** Fabrication control parameters.

| Laser Power (W) | Scan Speed (mm/s) | Distance Between Consecutive Laser Lines (mm) | Powder Feeding Rate (g/min) |
|---|---|---|---|
| 1000 | 10 | 0.7 | 3 |

The corrosion behavior of Al/SiC coatings on AA6082 aluminum alloy was evaluated. In addition, their corrosion behavior was compared with that of the uncoated substrate. Electrochemical measurements were made in an aerated 3.5 wt.% NaCl solution using an Autolab PGStat 30 (Metrohm AG, Herisau, Switzerland), exposing an area of 0.78 $cm^2$ of the sample to the test medium. All electrochemical tests were carried out at room temperature without stirring. A three-electrode cell was used for the electrochemical measurements; the working electrode was the own tested material and the counter and reference electrodes were graphite and silver/silver chloride (Ag/AgCl), respectively. A potential of ±20 mV around the corrosion potential ($E_{corr}$) with 1 mV/s scanning rate was applied for different immersion times in the electrolyte to calculate the polarization resistance ($R_p$). Anodic–cathodic polarization measurements were carried out at 0.005 V/s scan rate from −0.01 to 0.015 V with respect to $E_{corr}$. Tafel method was used to calculate the corrosion current density, according to ASTM standard G102 89 (1994) [27]. The corrosion products generated after immersion test were analyzed by a Scanning Electron Microscope (SEM) from Hitachi S3400N (Tokyo, Japan) equipped with an Energy Dispersive X-ray Spectrometer (EDS) from Brucker AXS X flash Detector 5010 (Billerica, MA, USA).

## 3. Results and Discussion

### *3.1. Coatings Microstructure*

The cross section of the different Al/$SiC_p$ coatings deposited on AA6082 by laser cladding is shown in Figure 1. SEM images of Al12Si/SiC, Al40Si/SiC and Al12Si20Ti/SiC are shown in Figure 1a–c, respectively. In all cases, a thick and continuous layer was deposited and a continuous metallurgical interface between substrate and coating can be observed. However, the microstructure of the different coatings shows many particularities, as it can be observed in the SEM images shown in Figure 2.

Al12Si/SiC microstructure (Figure 2a) main characteristic is the degradation of the $SiC_p$ reinforcement by the aluminum of the matrix. After the fabrication process the particles have lost their defined perimeter and show a serrated profile. It can also be observed the presence of $Al_4C_3$ platelets that appear as lines in the image and Si particles. This microstructure can be observed in other works [13,14,20]. In the Al40Si/SiC coating (Figure 2b), the SiC particles were not degraded and there was no presence of $Al_4C_3$. However, primary Si particles were observed [20]. These particles were formed because of the addition of Si as alloying element and not by the formation of Si because of the degradation of the $SiC_p$. Finally, the Al 12Si 20Ti/SiC microstructure was characterized by SiC particles, TiC and $TiSi_2$ in an Al-Si matrix (Figure 2c–d). Around the SiC particles, there was a characteristic Al inner ring and an outer TiC ring. The reason is that the Al reacts with SiC to form $Al_4C_3$ and Si. Also, Ti reacts with $SiC_p$ and forms TiC. In addition, Ti reacts with the Si and forms $TiSi_2$. [20]. The presence of these products in the composite matrix decreases the amount of the initial reinforcement, causing that in some cases, only a ring of TiC remains in the surroundings of a zone where a SiC particle existed is observed.

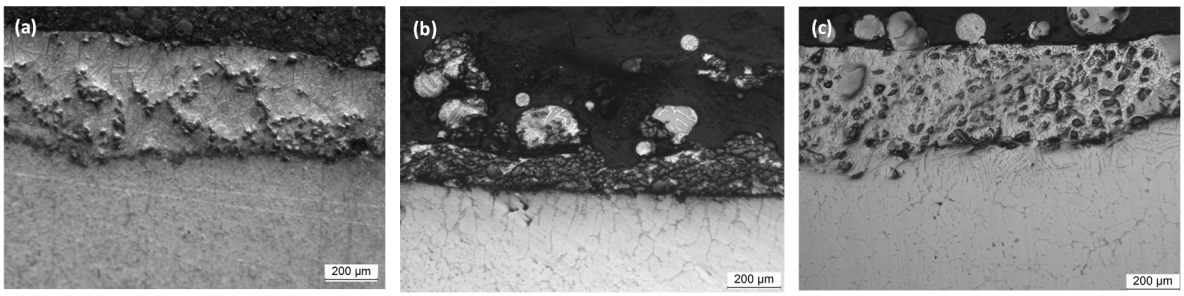


**Figure 1.** Cross section of the coatings deposited on the AA6082 alloy by laser cladding: (**a**) Al12Si/SiC; (**b**) Al40Si/SiC; (**c**) Al12Si-Ti/SiC.

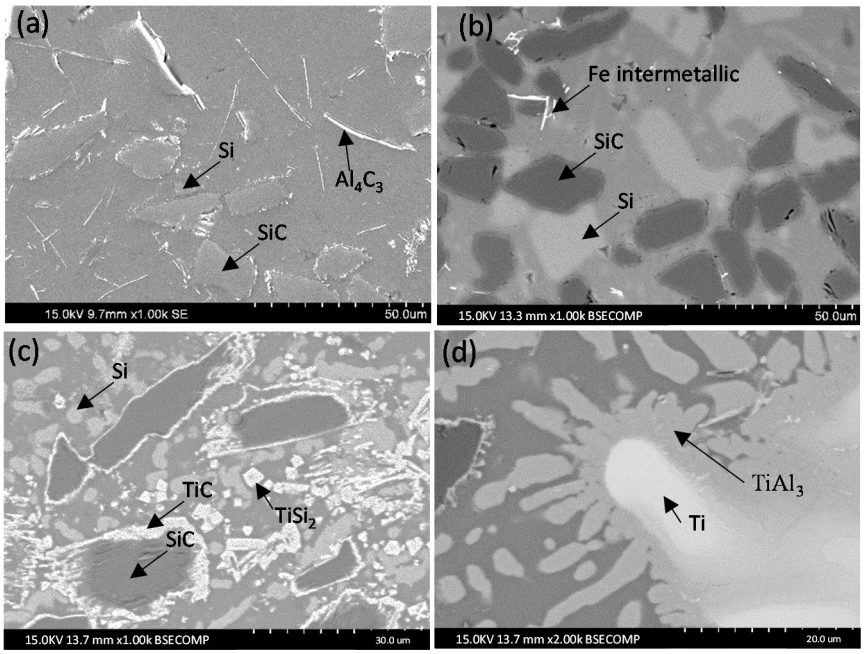


**Figure 2.** Microstructure of the coatings deposited on the AA6082 alloy: (**a**) Al12Si/SiC; (**b**) Al40Si/SiC; (**c**) Al12Si-Ti/SiC; (**d**) detail of the Al12Si-Ti/SiC.

### *3.2. Corrosion Properties*

The potentiodynamic anodic-cathodic polarization curves were obtained for different immersion times in 3.5% NaCl solution (1 h, 17 h, 24 h, 48 h, 72 h, 96 h and 168 h) for the uncoated AA6082 and Al12Si/SiC, Al40Si/SiC and Al12Si-20Ti/SiC coatings. Figure 3 resumes the main corrosion parameters obtained from the curves, i.e., the Open-circuit potential (OCP) and the corrosion current density, in Figure 3a,b, respectively. Polarization resistance was evaluated for the coatings at different immersion times (Figure 3c) and a gravimetric test was also made (Figure 3c).

Open-circuit potential (OCP) strongly varies with immersion time in the aggressive solution for all the systems (Figure 3a). For uncoated aluminum, $E_{corr}$ gradually increased for the first 72 h and for higher immersion times $E_{corr}$ kept constant. This can be explained by the formation of a superficial oxide layer that can partially protect the aluminum alloy from the corrosive effect of the chloride ions. In all coated systems, $E_{corr}$ showed a strong increase in the first hour of immersion, but then it decreased and for the first 48 h it showed instability and strong deviation between similar samples (large error bars). This behavior can be explained by the fast reaction between the species in the coatings with the corrosive media which would have formed a superficial oxide layer. However, the lack of homogeneity and stability of the coating may have caused its breaking and the strong changes observed in the behavior of the coatings. For long immersion times, the $E_{corr}$ values of the Al12Si/SiC coatings were similar to those of the AA6082 substrate, suggesting the formation of similar corrosion products However, the Al40Si/SiC coating was more active than AA6082 substrate, and Al12Si20Ti/SiC coating was nobler than the substrate. This indicates that the addition of Si or Ti, and the formation of different precipitated phases in this latter case, modifies the interaction of the coatings with the sodium chloride media.

The corrosion current density at OCP were measured under potentiostatically controlled conditions. Figure 3b shows the variation of corrosion current density with time for uncoated and Al/SiC coatings. For the first 24 h, the uncoated substrate had higher current density than the coated ones, indicating the occurrence of a fast anodic reaction. However for higher immersion times, the protective oxide layer formation increased its thickness, giving rise to a higher electrical resistance and a reduction in the corrosion current density, which kept nearly constant, suggesting that its thickness does not increase after the first 48 h of immersion. At the beginning of the experiment, the coatings that had nobler corrosion potentials, i.e.,Al12Si/SiC and Al12Si-Ti/SiC, had lower corrosion current densities than the substrate. Also,

for the first 24 h, they followed a similar behavior in which the current density decreased. Again, this suggests the formation of a protective layer. However, for higher immersion times, their behavior changes in function of their composition. Al12Si/SiC coating current density keep constant, but at 72 h, the current density increased steadily, indicating that the material is not capable of forming a protective oxide layer, and that corrosion is constantly progressing in the coating. The Al12Si-Ti/SiC coating current density kept constant for all times, although its values were higher than those of the AA6082 substrate. Finally, the current density of the Al40Si/SiC coating is lower than in the other systems for the first 24 h, but then it increased quickly indicating the presence of a speed anodic reaction.

Corrosion behavior of uncoated substrates and Al/SiC coatings was also studied in terms of the evolution of polarization resistance ($R_p$) with immersion time (Figure 3c). $R_p$ of the uncoated AA6082 increased in the first 24 h, again suggesting the formation of a superficial oxide protective layer which stabilized afterwards. The coated systems had a similar behavior, but the decreases observed in the evolution of $R_p$ suggest, again, the breaking of the protective superficial layer, which indicates that the oxide layers formed are not stable.

At the start of the experiment, nobler coatings (Al12Si/SiC and Al12Si-Ti/SiC) had higher $R_p$ values than uncoated AA6082 but at 24 h immersion time, the $R_p$ of the Al12Si/SiC decreased below that of the uncoated AA6082 and then kept constant. This indicates that there is a worse corrosion behavior than in the uncoated sample. Al40Si/SiC $R_p$ is lower than the uncoated AA6082 one, but it was constant for all immersion time. The Al12Si20Ti/SiC coating had the highest $R_p$ value, indicating that it had their best corrosion behavior. However the value oscillated throughout the immersion time, indicating, again, evolution in the structure of the oxide layer.

Figure 3d shows the mass gain of the samples with immersion time. In all cases, from 75 h mass increased. The Al12Si/SiC coating showed a nearly instant mass gain. Al40Si/SiC coating had the highest mass gain followed and the Al12Si20Ti/SiC had a similar mass gain than the uncoated AA6082. These behaviors can be explained by the species observed in the microstructure of the coatings. In the case of the Al12Si/SiC coating, $Al_4C_3$ was formed, but it is a very unstable compound that hydrates in the presence of humid environments, favoring the formation of different corrosion products. In the case of the Al40Si/SiC coating, the mass gain is associated with the large number of phases present, and therefore of interfaces, which act as preferred places of initial corrosion.

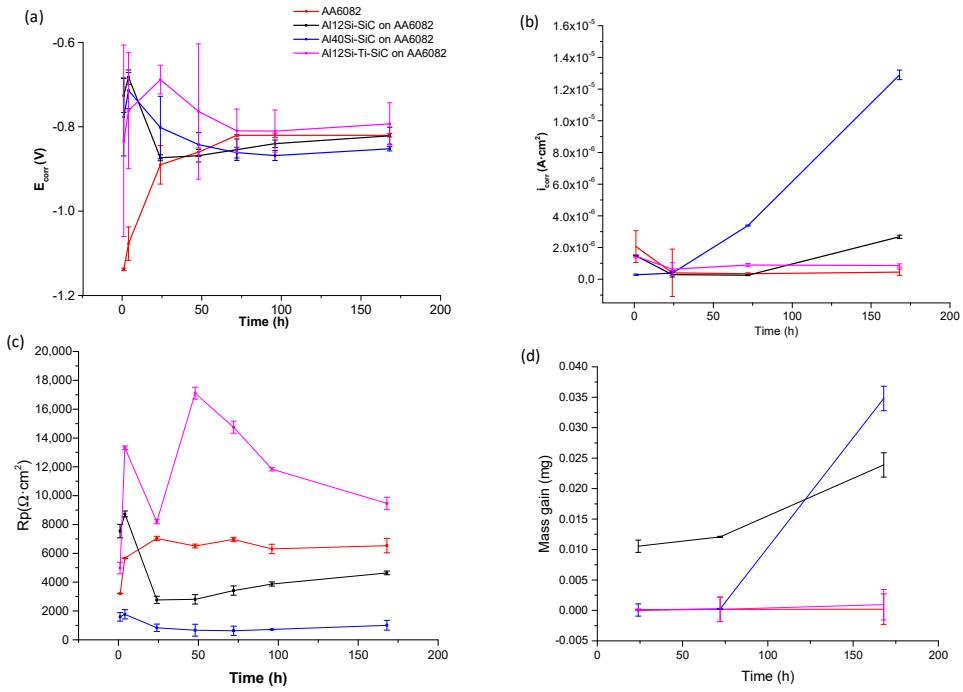

**Figure 3.** Corrosion values with time for the Al12Si/SiC, Al40Si/SiC, Al12Si-Ti/SiC coatings and for the uncoated AA6082 in 3.5% NaCl solution with time: (**a**) OCP measurement; (**b**) current density; (**c**) polarization resistance ($R_p$); and (**d**) mass gain.

### *3.3. Corrosion Products and Corrosion Mechanism*

Uncoated and coated samples were analyzed by SEM and EDS to identify the morphology and composition of the corrosion products when the materials were immersed in 3.5 wt.% NaCl at 25 °C for 168 h. The corrosion attack occurred in different ways in the different systems.

The AA6082 alloy substrate surface before the test surface is shown in Figure 4a. The surface morphology of uncoated AA6082 immersed in the test solution for 168 h is shown in Figure 4b. This surface presented generalized corrosion. A continuous layer of oxidized products was observed on the surface and the corrosion products were preferably deposited on the grinding peaks. A detail can be observed in Figure 4c and the EDS made on the surface shown in Figure 4d, revealed the presence of oxygen due to the presence of an oxidized layer (Figure 4e), which suggest that the corrosion products are mainly aluminum oxide.

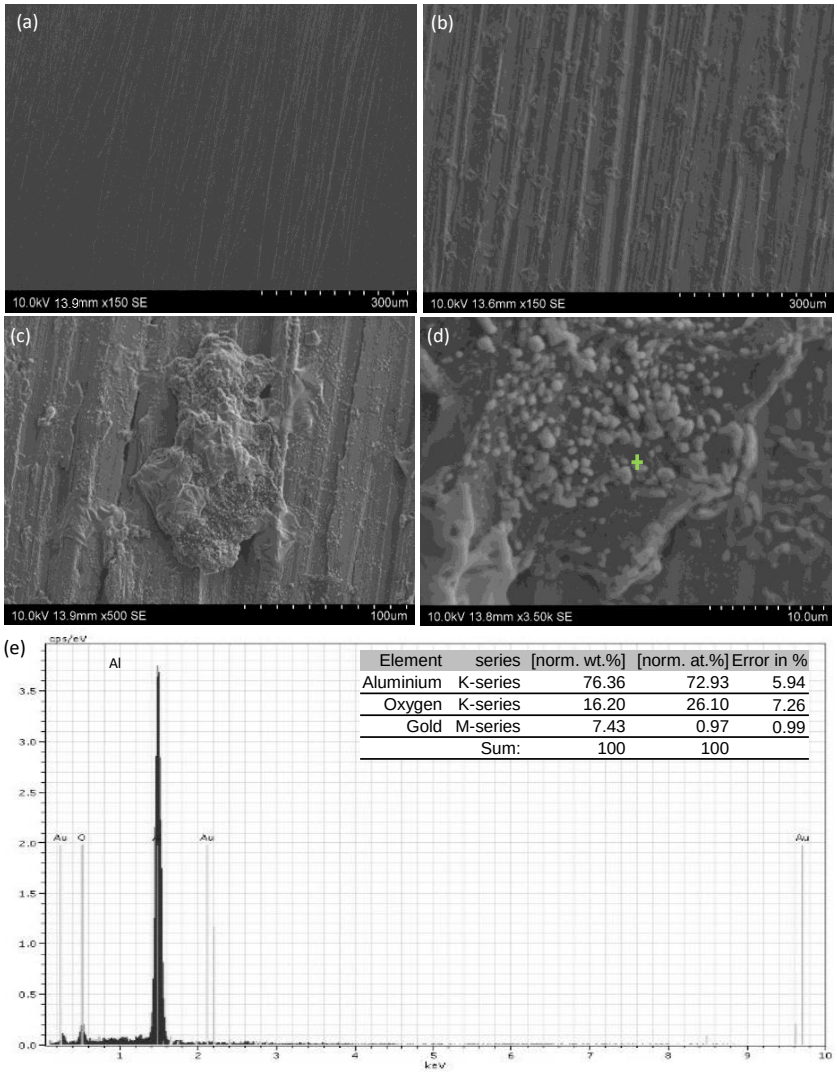


**Figure 4.** SEM images of the uncoated AA6082 alloy: (**a**) general view of surface before the immersion test in 3.5 wt.% NaCl; (**b**) general view after 168 h of immersion in 3.5 wt.% NaCl; (**c**) morphology of a corrosion product; (**d**) detail of (**c**); and (**e**) EDS analysis of zone marked in (**d**).

Al12Si/SiC coating corrosion surface is shown in Figure 5. A products layer with spongy appearance was formed in the surface (Figure 5a). A detail of the surface is shown in Figure 5b,c. The spongy corrosion products are mainly formed by oxygen and aluminum as determined by EDS (Figure 5d) made on the zone shown in Figure 5b. In some zones, this oxide layer broke and revealed the substrate surface as it is shown in Figure 5c. The EDS made on this zone reveal that these zones were rich in carbon, suggesting that it is caused by the presence of $Al_4C_3$.

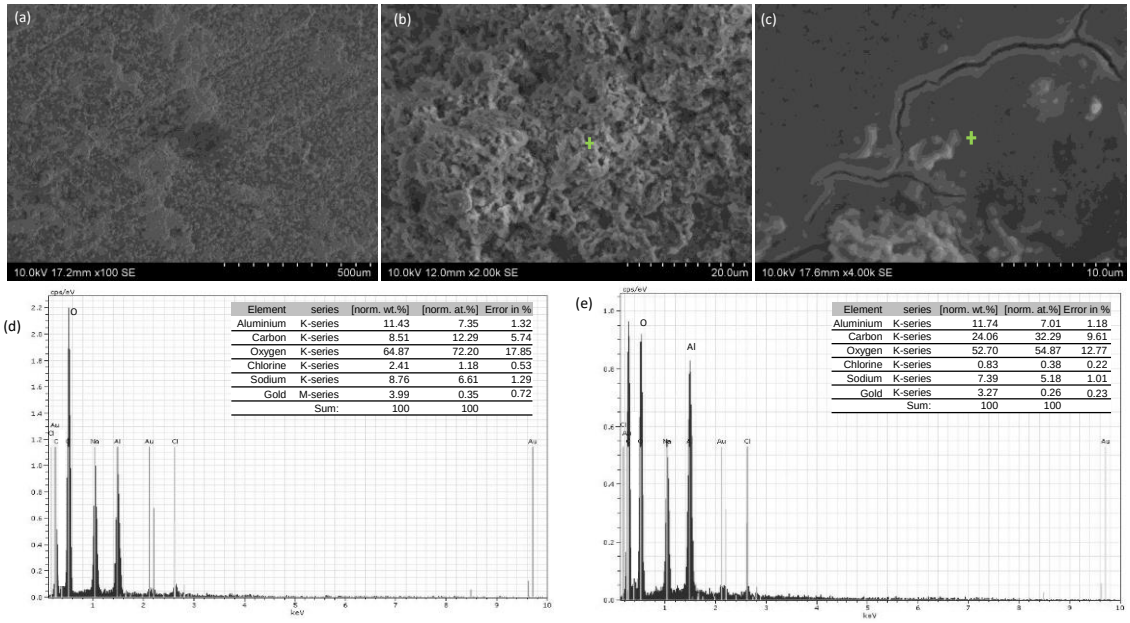


**Figure 5.** SEM images of the surface of the Al12Si/SiC coating after 168 h of immersion in 3.5 wt.% NaCl: (**a**) general view of surface; (**b**) and (**c**) details of the morphology of the corrosion products formed; general view; (**d**) and (**e**) EDS analysis of zones marked in (**b**) and (**c**), respectively.

Figure 6 shows the corroded surface of the Al40Si/SiC coating. Like in the Al12Si/SiC coating, in the Al40Si/SiC coating there was a spongy oxide products layer, although pitting corrosion was also observed (Figure 6a). In other zones, the corrosion products layer had broken as a result of localized attack by chlorides and the substrate surface beneath could be observed (Figure 6b). In these zones, signs of nucleation and growth of a new layer of oxidized products were also present. Figure 6c shows a detail of the surface in which the structure of the corrosion products can be seen. The EDS determined that the zones that conform the continuous corrosion products layer are mainly formed by oxygen and aluminum as determined by EDS (Figure 6d), being presumably $Al_2O_3$. In the zones were the coating has broken and in which localized corrosion is observed the EDS showed the presence of oxygen and silicon (e). These indicates that the zones in which these morphologies appear correspond with zones in which Si particles are located at the surface of the sample. Indicating that the presence of Si particles limits the formation of a continuous corrosion layer, and favors the attack by the $Cl^-$ ions.

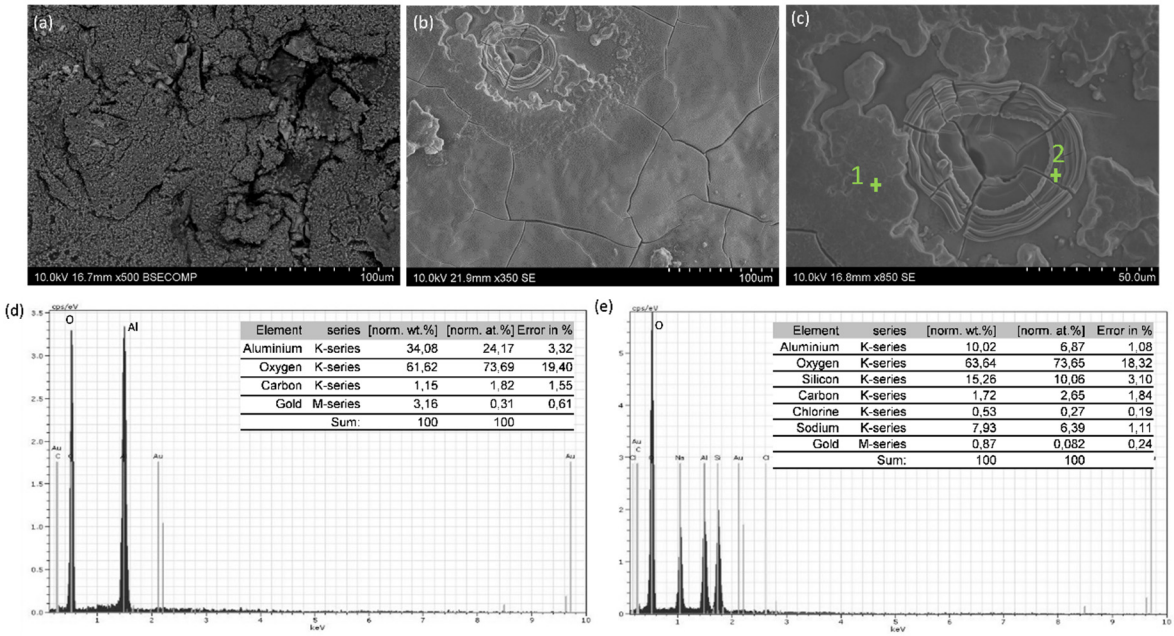


**Figure 6.** SEM images of the surface of the Al40Si/SiC coating after 168 h of immersion in 3.5 wt.% NaCl: (**a**) and (**b**) general view of two different zones of the surface; (**c**) detail of (b); (**d**) EDS analysis of point 1 in (**c**); and (**e**) EDS analysis of point 2 in (**c**).

Al12Si20Ti/SiC surface (Figure 7a) presents the same oxide products layer, although in this case the coating was less continuous, as it can be seen in the detail shown in Figure 7b. Cracked zones of the corrosion products layer (Figure 7c) and zones where pitting corrosion has taken place could be observed (Figure 7d). The EDS tests (Figure 7e,f) evidenced that the cracks formed because of pitting corrosion were formed in the vicinity of Ti rich zones, and the compositions observed correspond with $TiSi_2$ and $TiAl_3$. Therefore, it seems that the formation of the precipitates caused the appearance of microgalvanic couples which helped to the initiation and progression of corrosion in these coatings.

Figure 8 shows diagrams of the different corrosion mechanisms of the coating. The differences in the corrosion mechanism that the coatings present are conditioned by the quantity and nature of the phases present in each of them. In general, the localized attack on the aluminum matrix composite materials is favored by the irregularities of the passive layer of $Al_2O_3$, prior to the test, due to the presence of the reinforcement and intermetallic phases.

The phase-matrix interfaces act as areas where the $Cl^-$ ion can penetrate more easily, favoring a localized attack [28]. Pitting corrosion progresses through interfaces, grain boundaries, and stress concentration zones. In these zones, the $Cl^-$ ion reacts with the passive alumina layer, forming soluble species that dissolve the layer, leaving the alloy exposed to the medium. The hydrolysis of the $Al^{3+}$ cation occurs, which causes a decrease in the pH of the medium due to the formation of acidic species, such as $AlCl_3$ and $H^+$ according to the reactions [29,30]. A porous layer of corrosion products accumulates on the surface of the sample, such as $Al_2O_3{\cdot}3H_2O$ (bayerite) and AlO(OH), whose nature has been determined by other authors in similar materials [31].

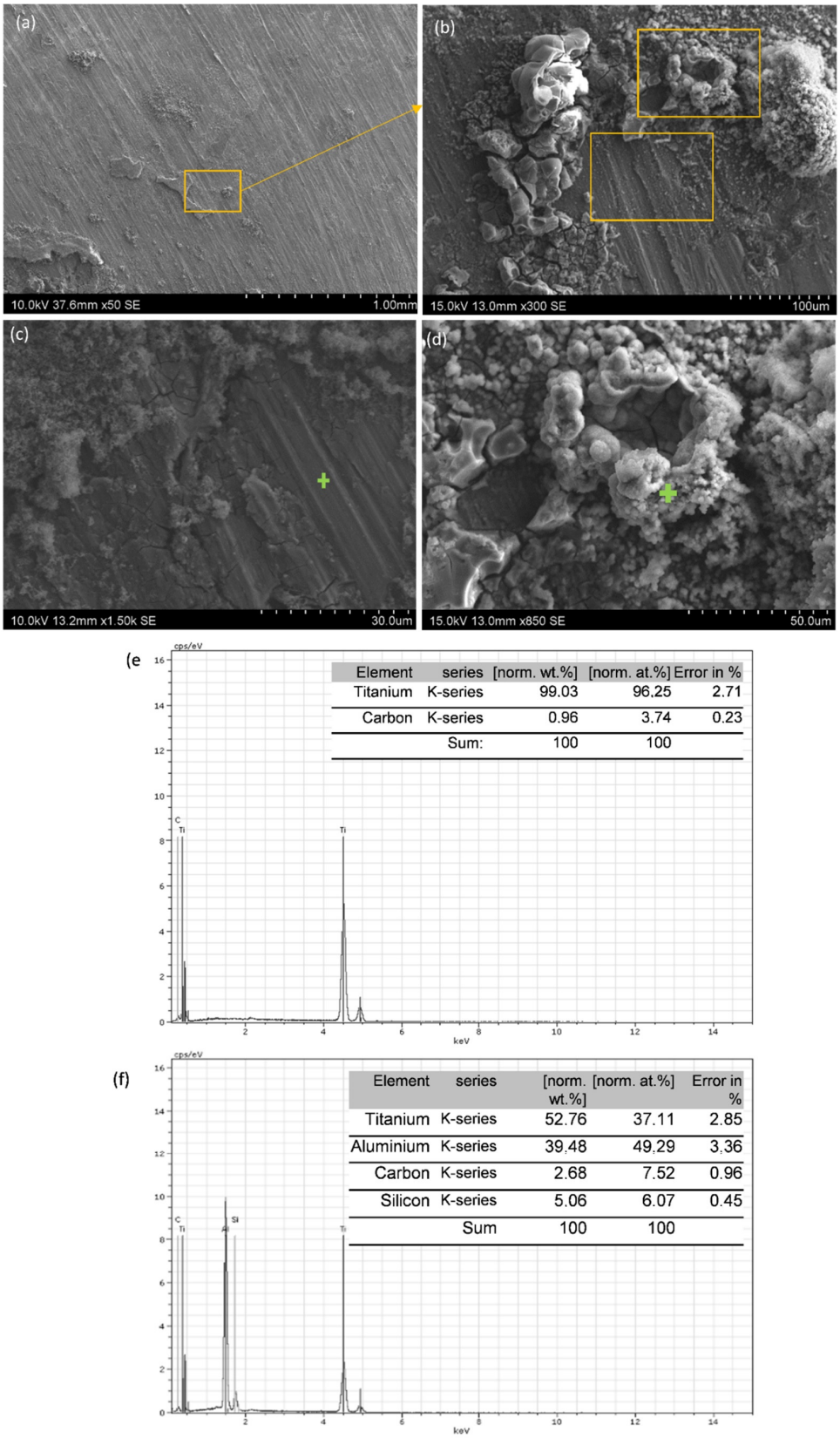


**Figure 7.** SEM images of the surface of the Al12Si20Ti/SiC coating after 168 h of immersion in 3.5 wt.% NaCl: (**a**) general view; (**b**) detail of the morphology of the coating; (**c**,**d**) details of (**b**); (**e**) EDS analysis of point marked in (**c**); and (**f**) EDS analysis of point marked in (**d**).

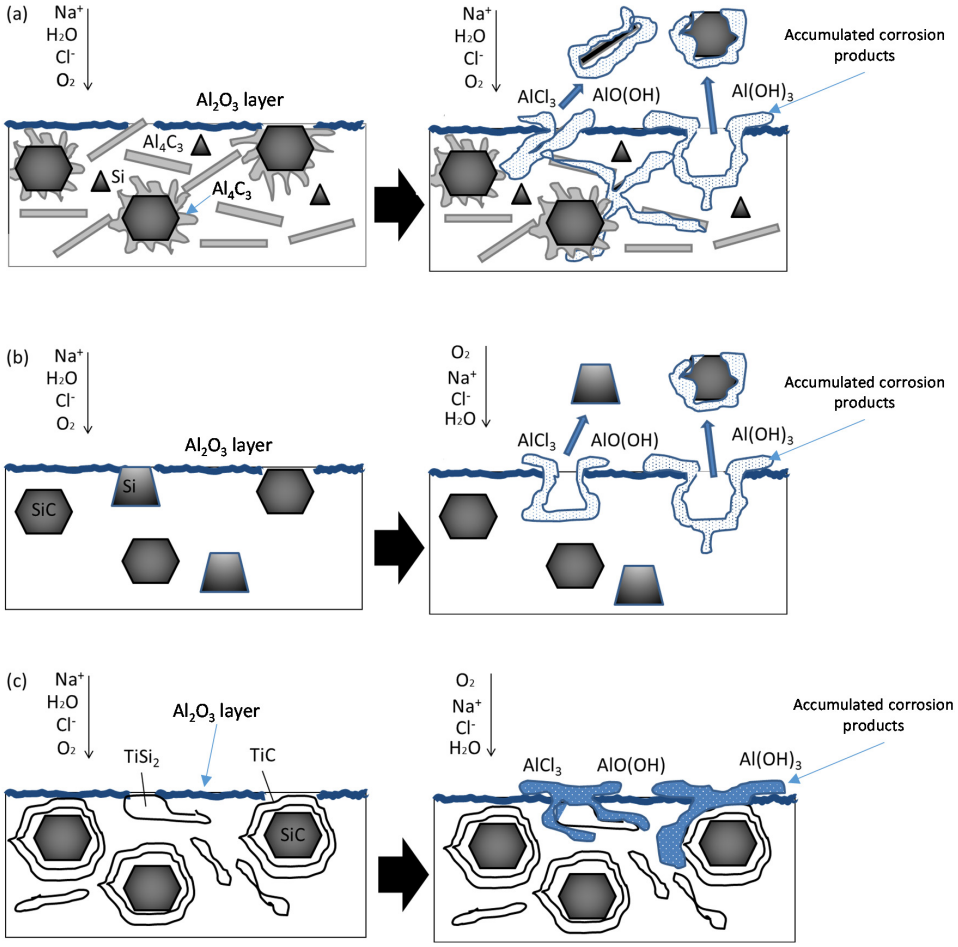


**Figure 8.** Corrosion mechanisms scheme in the surface of the different coatings: (**a**) Al12Si/SiC; (**b**) Al40Si/SiC; (**c**) Al12Si-Ti/SiC coating surface.

In the case of the Al12Si/SiC coating (Figure 8a), in addition to the reinforcement and the intermetallic phases, the presence of aluminum carbide was observed. This carbide greatly influences the corrosion behavior of this type of materials, since in the presence of humid environments it hydrates and forms aluminum hydroxide according to reaction (5), which increases its volume and causes the oxide layer breaks, which accelerates the corrosion process in its vicinity [32].

$$Al^{3+} + 3H_2O \leftrightarrows Al(OH)_3 + 3H^+ \quad (1)$$

$$2Al + 4H_2O \leftrightarrows 2AlO(OH) + 3H_2 \quad (2)$$

$$Al_2O_3 + 2nCl^- + 6H^+ \leftrightarrows 2AlCl_n^{(3-n)+} + 3H_2O \quad (3)$$

$$O_2 + 2H_2O + 4e^- \leftrightarrows 4OH^- \quad (4)$$

$$Al_4C_3 + 12\ H_2O \leftrightarrows 4Al(OH)_3 + 3\ CH_4 \quad (5)$$

Al40Si/SiC corrosion mechanism is shown in Figure 8b. This material does not have $Al_4C_3$, so a fast degradation of the material does not take place. However, there is a large amount of Si in form of big particles, apart from $SiC_p$ itself. This causes that there was a great irregularity in the oxidized layer formed, as it is not equally formed in the particles and in the aluminum, and there was also a large number of interfaces. Silicon-rich zones and SiC particles act as preferential pitting zones and the corrosion progresses through the interfaces producing the detachment of some of them and promoting

the advancement of pitting. Preferential accumulation of circular corrosion products occurs around active pitting when the particle has been removed.

Figure 8c shows the corrosion mechanism that takes place in the Al12Si-Ti/SiC system. The oxide layer is less discontinuous than in the previous cases, since there are fewer phases that are prone to the attack by the humid environment or by the chloride ions. The interfaces between the matrix and the precipitated phases observed, i.e., $TiSi_2$, $TiAl_3$ and TiC, are zones of discontinuities on the oxide layer and they are the only zones in which the degradation occurs. The formation of oxides in the form of a chimney is associated with the accumulation of corrosion products around the pit, which continues to be active while the transport of $O_2$ into it is possible.

## 4. Conclusions

The corrosion behavior of different composition Al/SiC composite coatings on AA6082 aluminum alloy have been evaluated in 3.5 wt.% NaCl solution for 168 h. At long immersion times (>168 h) Al12Si/SiC coating on AA6082 presents similar corrosion behavior than the AA6082 substrate. Al40Si/SiC are more active than the substrate and Al12Si-Ti/SiC are nobler than the others including the aluminum substrate.

The main corrosion products are, in all cases, oxyhydroxides, $Al(OH)_3$ and $Al_2O_3$, however the corrosion mechanisms are different in function of the coating composition. The failures of the protective nature of the coatings are due to the presence of discontinuities on the surface corrosion products layer. In the case of the Al12Si/SiC coating the discontinuities are SiC particles, $Al_4C_3$ platelets and intermetallic phases. Primary silicon are the main discontinuities in Al14Si/SiC coating. And, in the case of Al12Si-Ti/SiC the corrosion advances through the discontinuities formed by $TiSi_2$, $TiAl_3$ and TiC.

**Author Contributions:** Investigation, A.R.; writing—original draft, A.R.; writing—review & editing, P.R., M.D.E.-R., and J.R. All authors have read and agreed to the published version of the manuscript.

**Funding:** This research was funded by Comunidad de Madrid (ADITINANO and ADITIMAT-CM S2018/NMT-4411), Agencia Estatal de Investigación (RTI 2018-0963-B-C31) and Universidad Rey Juan Carlos (2020/00006/004).

**Conflicts of Interest:** The authors declare no conflict of interest. The funders had no role in the design of the study; in the collection, analyses, or interpretation of data; in the writing of the manuscript, or in the decision to publish the results.

## References

1. Dubourg, L.; Ursescu, D.; Hlawka, F.; Cornet, A. Laser cladding of MMC coatings on aluminum substrate: Influence of composition and microstructure on mechanical properties. *Wear* **2005**, *258*, 1745–1754. [CrossRef]
2. Bodunrin, M.O.; Alaneme, K.K.; Chown, L.H. Aluminum matrix hybrid composites: A review of reinforcement philosophies; mechanical, corrosion and tribological characteristics. *J. Mater. Res. Technol.* **2015**, *4*, 434–445. [CrossRef]
3. Zhang, L.; Xu, H.; Wang, Z.; Li, Q.; Wu, J. Mechanical properties and corrosion behavior of Al/SiC composites. *J. Alloys Compd.* **2016**, *678*, 23–30. [CrossRef]
4. Sulaiman, S.; Marjom, Z.; Ismail, M.I.S.; Ariffin, M.K.A.; Ashrafi, N. Effect of Modifier on Mechanical Properties of Aluminum Silicon Carbide (Al-SiC) Composites. *Procedia Eng.* **2017**, *184*, 773–777. [CrossRef]
5. Riquelme, A.; Rodrigo, P.; Escalera-Rodríguez, M.D.; Rams, J. Analysis and optimization of process parameters in Al-SiCp laser cladding. *Opt. Lasers Eng.* **2016**, *78*, 165–173. [CrossRef]
6. Riquelme, A.; Escalera-Rodríguez, M.D.; Rodrigo, P.; Rams, J. Role of Laser Cladding Parameters in Composite Coating (Al-SiC) on Aluminum Alloy. *J. Therm. Spray Technol.* **2016**, *25*, 1177–1191. [CrossRef]
7. Arunkumar, S.; Subramani, S.M.; Suketh, K.K.M.; Vigneshwara, S. A review on aluminium matrix composite with various reinforcement particles and their behaviour. *Mater. Today Proc.* **2020**, in press. [CrossRef]
8. Sivananthan, S.; Ravi, K.C.; Samuel, S.-J. Effect of SiC particles reinforcement on mechanical properties of aluminium 6061 alloy processed using stir casting route. *Mater. Today Proc.* **2020**, *21*, 968–970. [CrossRef]
9. Bienia, J.; Walczak, M.; Surowska, B.; Sobczaka, J. Microstructure and corrosion behaviour of aluminum fly ash composites. *J. Optoelectron. Adv. Mater.* **2003**, *5*, 493–502.

10. Yao, J.; Zhang, W.J.; Wang, G.L.; Zhang, Q.; Liu, R. Microstructure and wear resistance of laser cladded composite coatings prepared from pre-alloyed WC-NiCrMo powder with different laser spots. *Opt. Laser Technol.* **2018**, *101*, 520–530. [CrossRef]
11. Jiao, X.; Wang, C.; Gong, Z.; Wang, G.; Sun, H.; Yang, H. Effect of Ti on T15M composite coating fabricated by laser cladding technology. *Surf. Coat. Technol.* **2017**, *325*, 643–649. [CrossRef]
12. Gao, T.; Wang, D.; Du, X.; Li, D.; Liu, X. Phase transformation mechanism of $Al_4C_3$ by the diffusion of Si and a novel method for in situ synthesis of SiC particles in Al melt. *J. Alloys Compd.* **2016**, *685*, 91–96. [CrossRef]
13. Rams, J.; Ureña, A.; Campo, M. Dual layer silica coatings of SiC particle reinforcements in aluminum matrix composites. *Surf. Coat. Technol.* **2006**, *200*, 4017–4026. [CrossRef]
14. Ureña, A.; Escalera, M.D.; Gil, L. Influence of interface reactions on fracture mechanisms in TIG arc-welded aluminum matrix composites. *Compos. Sci. Technol.* **2000**, *60*, 613–622. [CrossRef]
15. Vreeling, J.A.; Ocelík, V.; Pei, Y.T.; Van Agterveld, D.T.L.; De Hosson, J.T.M. Laser melt injection in aluminum alloys: On the role of the oxide skin. *Acta Mater.* **2000**, *48*, 4225–4233. [CrossRef]
16. Anandkumar, R.; Almeida, A.; Colaco, R.; Vilar, R.; Ocelik, V.; De Hosson, J.T.M. Microstructure and wear studies of laser clad Al-Si/SiC(p) composite coatings. *Surf. Coat. Technol.* **2007**, *201*, 9497–9505. [CrossRef]
17. Han, P.N.; Stevens, G.R. Interfacial structure and fracture of aluminum alloy A356-SiC particle metal matrix composite. *Mater. Sci. Technol.* **1992**, *8*, 184–188. [CrossRef]
18. Anandkumar, R.; Almeida, A.; Colaço, R.; Vilar, R.; Ocelik, V.; De Hosson, J.T.M. Influence of powder particle injection velocity on the microstructure of Al-12Si/SiCp coatings produced by laser cladding. *Surf. Coat. Technol.* **2009**, *204*, 285–290. [CrossRef]
19. Zheng, B.J.; Chen, X.M.; Lian, J.S. Microstructure and wear property of laser cladding Al + SiC powders on AZ91D magnesium alloy. *Opt. Laser. Eng.* **2010**, *48*, 526–532. [CrossRef]
20. Riquelme, A.; Escalera-Rodríguez, M.D.; Rodrigo, P.; Otero, E.; Rams, J. Effect of alloy elements added on microstructure and hardening of Al/SiC laser clad coatings. *J. Alloys Compd.* **2017**, *727*, 671–682. [CrossRef]
21. Viala, Y.; Bosselet, J.C.; Laurent, F.; Lepetitcorps, V. Mechanism and kinetics of the chemical interaction between liquid aluminum and silicon-carbide single crystals. *J. Mater. Sci.* **1993**, *28*, 5301–5312. [CrossRef]
22. Lloyd, D.J. Particle reinforced aluminum and magnesium matrix composites. *Int. Mater. Rev.* **1994**, *39*, 1–23. [CrossRef]
23. Lee, J.C.; Park, S.B.; Seok, H.K.; Oh, C.S.; Lee, H.I. Prediction of Si contents to suppress the interfacial reaction in the SiCp/2014 Al composite. *Acta Mater.* **1998**, *46*, 2635–2643. [CrossRef]
24. Wu, H.; Cui, X.P.; Geng, L.; Fan, G.H.; Pang, J.C.; Wei, L.S. Fabrication and characterization of in-situ TiAl matrix composite with controlled microlaminated architecture based on SiC/Al and Ti system. *Intermetallics* **2013**, *43*, 8–15. [CrossRef]
25. Lü, X.H.; Yang, Y.Q.; Liu, C.X.; Yan, C.H.E.N.; Ai, Y.L. Kinetics and mechanism of interfacial reaction in SCS-6 Sic continuous fiber-reinforced Ti-A1 intermetallic matrix composites. *Trans. Nonferrous Met. Soc. China* **2006**, *16*, 77–83. [CrossRef]
26. Schuster, J.C.; Palm, M. Reassessment of the binary Aluminum-Titanium phase diagram. *J. Phase Equilibria Diffus.* **2006**, *27*, 255–277. [CrossRef]
27. *Calculation of Corrosion Rates & Related Information from the Electrochemical Measurements*; ASTM standard G102 89; ASTM: West Conshohocken, PA, USA, 1994.
28. Loto, R.T.; Babalola, P. Corrosion resistance of low SiC particle variation at low weight content on 1060 aluminum matrix composite in sulfate-contaminated seawater. *Results Phys.* **2019**, *13*, 102241. [CrossRef]
29. Zamri, Y.B.; Shamsul, J.B.; Ahmad, K.R. Corrosion of aluminium matrix composites. In Proceedings of the National Metallurgical Conference 2006, Kangar, Perlis, Malaysia, 9–10 December 2006. [CrossRef]
30. Pyun, S.I.; Moon, S.M.; Ahn, S.H.; Kim, S.S. Effects of $Cl^-$, $NO^-_3$ and $SO^{2-}_4$ ions on anodic dissolution of pure aluminum in alkaline solution. *Corros. Sci.* **1999**, *41*, 653–667. [CrossRef]
31. Ureña, A.; Otero, E.; Utrilla, M.V.; Rodrigo, P. Mecanismos de corrosión en materiales compuestos de matriz de aluminio con refuerzo de SiC. *Bol. Soc. Esp. Ceram. Vidr.* **2004**, *43*, 233–236. [CrossRef]
32. Holleman, A.F. *A Text-Book of Organic Chemistry*; John Wiley & Sons: New York, NY, USA, 1907; p. 36.


coatings

an Open Access Journal by MDPI

CITESCORE 2.4 SCOPUS

IMPACT FACTOR 2.436

# CERTIFICATE OF PUBLICATION

Certificate of publication for the article titled:

Corrosion Resistance of Al/SiC Laser Cladding Coatings on AA6082

Authored by:

Ainhoa Riquelme; Pilar Rodrigo; María Dolores Escalera-Rodríguez; Joaquín Rams

Published in:

*Coatings* **2020**, Volume 10, Issue 7, 673

MDPI Academic Open Access Publishing since 1996

Basel, July 2020